

# The influence of fuelbed properties on moisture drying rates and timelags of longleaf pine litter

Ralph M. Nelson Jr. and J. Kevin Hiers

**Abstract:** Fire managers often model pine needles as 1 h timelag fuels, but fuelbed properties may significantly change the rate at which needles exchange moisture with the atmosphere. The problem of determining whether moisture loss from fine fuels is being controlled by individual particles or by the fuelbed remains unresolved. Results from this laboratory experiment indicate that first-period timelags of longleaf pine (*Pinus palustris* Mill.) needles are altered by fuelbed loading and needle arrangement. Timelags of individual needles ranged from 3.3 to 5.3 h; timelags of beds of vertically oriented needles (4.4 to 8.6 h) approximated those of individual particles, but were slightly influenced by loading. Beds of horizontal needles dried with load-dependent timelags that varied from 6.5 to 31.6 h. Fuel loads ranged from 0.04 (for individual particles) to 1.07 kg·m<sup>-2</sup>. We report a new metric, the area drying rate, which is analogous to a unit-area burning rate. For beds of flat needles, plots of the area drying rate versus fuel load illustrate a transition from control by individual particles to control by the bed structure when fuel loading is approximately 0.33 kg·m<sup>-2</sup>. Beds of vertical needles were particle controlled. Results should be useful to fire managers when modeling fire behavior.

**Résumé :** Les gestionnaires du feu modélisent souvent les aiguilles de pin en assumant qu'il s'agit d'un combustible dont le temps de séchage est d'une heure mais les propriétés des couches de combustibles peuvent modifier de façon significative le taux d'échange d'humidité des aiguilles avec l'atmosphère. La question qui consiste à savoir à quel moment la perte d'humidité des combustibles légers est déterminée par les particules individuelles ou la couche de combustibles demeure sans réponse. Les résultats de cette expérience en laboratoire indiquent que le temps de séchage de la première période des aiguilles de pin des marais (*Pinus palustris* Mill.) est influencé par la charge de la couche de combustibles et l'arrangement des aiguilles. Le temps de séchage des aiguilles individuelles varie de 3,3 à 5,3 h; le temps de séchage des couches de combustibles où les aiguilles sont orientées verticalement correspond approximativement à celui des particules individuelles mais il est légèrement influencé par la charge de combustibles. Les couches de combustibles où les aiguilles sont placées à l'horizontal ont un temps de séchage de 6,5 à 31,6 h dépendamment de la charge de combustibles. La charge de combustibles varie de 0,04 (pour les particules individuelles) à 1,07 kg·m<sup>-2</sup>. Nous présentons une nouvelle mesure, la vitesse de séchage en surface, qui est analogue à la vitesse de combustion en surface. Pour les couches de combustibles où les aiguilles sont à plat, la représentation graphique de la vitesse de séchage en surface en fonction de la charge de combustibles illustre la transition entre le moment où la perte d'humidité est déterminée par les particules individuelles et celui où elle est déterminée par la structure de la couche de combustibles lorsque la charge de combustibles atteint approximativement 0,33 kg·m<sup>-2</sup>. Dans les couches de combustibles où les aiguilles sont placées à la verticale, la perte d'humidité est déterminée par les particules. Les résultats devraient être utiles aux gestionnaires du feu pour modéliser le comportement du feu.

[Traduit par la Rédaction]

## Introduction

Moisture exchange between fine dead fuels and the atmosphere is a fundamental process affecting fire behavior predictions, but the influence of fuelbed structure on the rate of exchange remains uncertain (Anderson 1990). Investigators of fire behavior (Weber and De Mestre 1990; Lyons and Weber 1993) have studied the influence of fuel-particle ori-

entation on rate of fire spread but, to our knowledge, the only wildland fuel moisture study that includes fuelbeds with differing particle orientations is that of Anderson (1990). In his work, Anderson reports timelags for moisture loss and gain in 18 fine forest fuels, including cheatgrass (*Bromus tectorum* L.) beds in which individual particles were standing vertically to represent cheatgrass in situ. His data indicate that for adsorption and desorption in recently cast fuels, only cheatgrass and witch's hair (*Alectoria jubata* L.) exhibit timelags of 1 h or less. Anderson's data highlight the need for a better understanding of the influence of the characteristics of individual particles, fuelbed structure, and fuel loading on moisture relationships. Such information should lead to improved systems of fire danger rating and fire behavior prediction.

Several applications of diffusion theory have been used to describe the drying of forest fuels (Linton 1962; Byram 1963; Nelson 1969; Fosberg 1975; Van Wagner 1979; Anderson 1990; Viney 1992). Solutions of the diffusion

Received 11 February 2008. Accepted 10 May 2008. Published on the NRC Research Press Web site at cjfr.nrc.ca on 19 August 2008.

**R.M. Nelson, Jr.** Joseph W. Jones Ecological Research Center, Route 2, Box 2324, Newton, GA 39870, USA; USDA Forest Service (retired), 206 Morning View Way, Leland, NC 28451, USA.

**J.K. Hiers.**<sup>1</sup> Joseph W. Jones Ecological Research Center, Route 2, Box 2324, Newton, GA 39870, USA.

<sup>1</sup>Corresponding author (e-mail: khiers@jonesctr.org).

equation for various fuel particles often are compared with data from laboratory experiments in which fuelbed drying occurs at constant room temperature and relative humidity and with normal air circulation. Fosberg (1975, 1977) presented a physical description of litter-bed drying in terms of mass and energy conservation. An important point in his discussion is that the drying of litter beds is controlled by the drying rates of fuel particles. In his study of response times of western fuels, Anderson (1990) discussed the dilemma of whether fuelbed drying is controlled by particle properties or bed properties. Following Fosberg (1975), he computed moisture diffusivities for his experimental fuelbeds using particle radius rather than fuelbed thickness. However, Anderson states that “the equations developed to estimate response time to  $E_{63}$  include the fuel bed thickness and the fuel bed packing ratio...Other fuel bed geometries may cause additional variation, such as matted cheatgrass rather than standing cheatgrass. Just how open a fuel bed must be for the particle thickness to be the controlling thickness property will require additional study.” Note that Anderson (1990) used “ $E_{63}$ ” when referring to a fuelbed moisture loss equal to 63% of the total water available for loss during a drying run.

We are not aware of further research concerning the question of particle- versus bed-controlled drying. The experiments reported in this paper, initially devoted to the effects of fuel-particle arrangement on drying rate, presented an opportunity to briefly study the drying-control question and to inquire whether there exists a fuelbed parameter that indicates transition from drying control by particles to fuelbed control as the parameter's value increases. In a study of the reaction times of laboratory head fires in four different fuels, including ponderosa pine (*Pinus ponderosa* Dougl. ex Laws.) needle beds, Nelson (2003) observed two combustion regimes when the unit-area burning rate (mass loss rate per unit planar area of bed) was graphed as a function of the fuel-load parameter (square metres of fuel particle surface per square metre fuelbed planar area). Area fires in wooden cribs produce comparable results (Block 1971). The loss of water from pine needle beds during drying may be similar (in a gross sense) to the loss of volatiles during heading fires and area fires in laboratory-scale fuelbeds. Thus our purpose in studying the effects of fuel loading and arrangement on the timelag and the area drying rate (defined below) is to determine whether two regimes similar to the burning regimes in ponderosa pine needle beds are observed during the drying of longleaf pine (*Pinus palustris* Mill.) needles. We derive an area drying rate analogous to the unit-area burning rate and interpret the experimental data in terms of the fuel-load parameter (also defined below).

## Drying concepts

### Heat-mass transfer, particle orientation, timelag periods

The similarities between heat transfer and mass transfer are documented in many texts (e.g., Kreith 1967; Incropera and DeWitt 1996). For a long, thin cylindrical solid that is warmer than its surroundings and oriented vertically, the free-convection flow is driven by a temperature difference between the solid and its surroundings, or equivalently, by differences in air density. If the solid is oriented horizontally

under otherwise identical conditions, the processes taking place are similar, though heat flow to the surroundings will be slightly smaller than it is for the vertical orientation (Holman 1990). On the other hand, a vertically oriented pine needle at room temperature often holds an amount of water greater than the amount it would hold when it is in thermodynamic equilibrium with its surroundings, inducing the process analogous to cooling, i.e., that of drying.

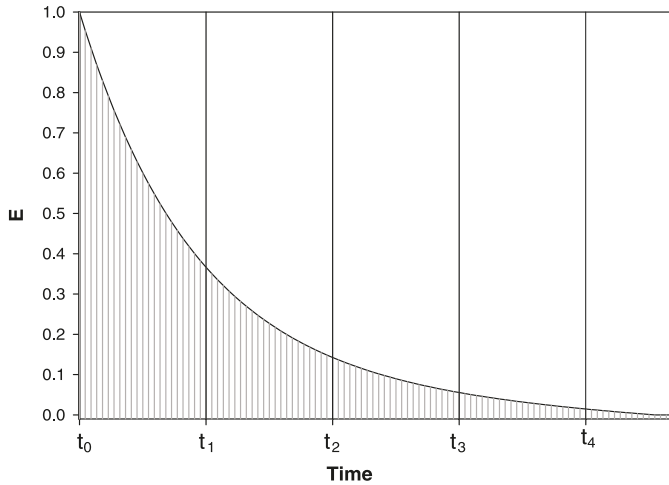
The drying process in forest fuels such as pine needles is more complex than cooling of the solid described above because the initial drying mechanism is determined by the moisture content of the needles. For instance, when free water is held on the surface and in the air spaces of the needle, drying initially occurs through evaporation — a process in which the needle temperature decreases a few degrees because the energy required for evaporation is supplied by the needle. This process has no counterpart in the above example of the cooling solid. When the transfer rate of internal free water to the needle surface becomes slower than the potential rate at which water could be evaporated at the surface under the prevailing conditions, the drying mechanism changes because the surface begins to dry. Water moves at a relatively slow rate to the needle surface and into the adjacent air by the combined diffusion of bound water and water vapor (Van Wagner 1979; Nelson 2001). The resulting flow of vapor is due to density differences between the vapor in air adjacent to the needle surface and the vapor in the surrounding air. If we now consider a bed composed of many needles, water loss from the bed will be driven by the mean difference between vapor pressures in the bed interior and vapor pressure in the external air. For the present drying experiments, we expect to observe results similar to those for heat transfer (i.e., drying is slower when wet needles are oriented horizontally rather than vertically, and ambient conditions do not change).

According to the timelag theory presented by Byram (1963), the drying of forest fuels (particles or beds) in constant ambient conditions can be described with the following exponential decay equation

$$[1] \quad E = \frac{m - m_e}{m_0 - m_e} = \exp\left(\frac{-t}{\tau}\right)$$

where  $E$  is the fraction of evaporable water remaining in the fuelbed at time  $t$  (hours),  $m$  (kilograms per kilogram) is the average fractional moisture content in the particle or bed at  $t$ ,  $m_0$  is the value of  $m$  at  $t = 0$ ,  $m_e$  is the value of  $m$  as  $t$  approaches infinity ( $m$  approaches the equilibrium fractional moisture content), and  $\tau$  (hours) is the moisture timelag (theoretically constant within an entire drying run). For a laboratory run in which the fuelbed dries from  $m_0$  to  $m_e$ , the time required for  $E$  to decrease from unity to  $e^{-1}$  (or 0.368) is referred to as the response time or timelag; other less frequently used terms are timelag constant or log drying rate (Nelson 1969; Van Wagner 1969). Equation 1 implies that moisture remaining in the sample follows an exponential decay during the entire drying process. Evidence in the literature is not clear on this point. Several investigators (Anderson et al. 1978; Van Wagner 1979) show that deviations from the exponential relationship occur during the drying of forest fuels in the laboratory. On the other hand, Van Wagner (1982) states that drying jack pine (*Pinus banksiana*

**Fig. 1.** Timelag periods determined from a plot of moisture content fraction,  $E$ , versus time,  $t$ . The four drying periods correspond to  $E = 0.368, 0.135, 0.050,$  and  $0.018,$  respectively. The first-period timelag occurs at the value  $E = 0.368$ .



Lamb.) and white pine (*Pinus strobus* L.) needles follow the exponential form closely and show no significant dependence on initial moisture content,  $m_0$ .

In a typical laboratory drying experiment, fuelbed mass data (kilograms) are recorded as a function of time  $t$ . Moisture content  $m = m(t)$  represents the average moisture content of the bed expressed as a fraction of the bed oven-dry mass,  $M_{od}$  (kilograms). From the initial and final bed masses and  $M_{od}$ , the initial and equilibrium fractional moisture contents  $m_0$  and  $m_e$  can be calculated. Thus the maximum evaporable moisture content is  $(m_0 - m_e)$ , and the fraction of evaporable water in the bed at time  $t$  is  $E = E(t) = (m - m_e)/(m_0 - m_e)$ . Anderson et al. (1978) describe timelag periods using  $E$  values equal to  $e^{-1}$  (0.368),  $e^{-2}$  (0.135),  $e^{-3}$  (0.050), etc. (Fig. 1). Thus the data points  $(0, 1)$  and  $(t_1, e^{-1})$  define the first-period timelag as  $\tau_1 = (t_1 - 0) = t_1$ ; the second-period timelag is defined by the data points  $(t_1, e^{-1})$  and  $(t_2, e^{-2})$ , with  $\tau_2 = (t_2 - t_1)$ , etc. In this paper, we determine only the first-period timelags and corresponding drying rates; thus the subscript 1 is subsequently omitted. The mean first-period drying rate,  $R_m$  (kilograms per hour), is

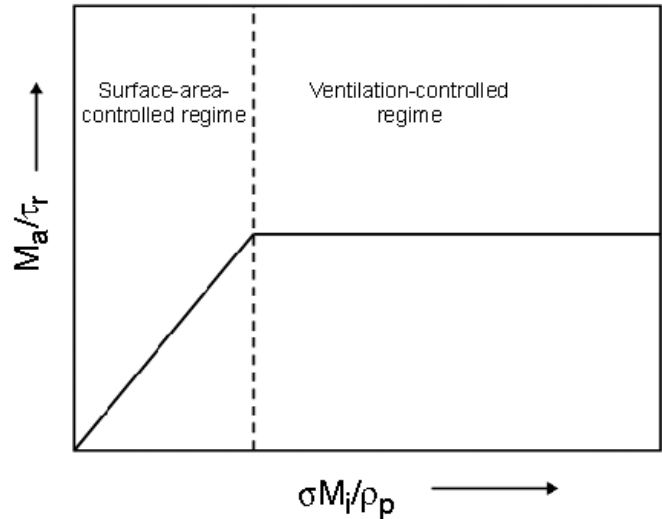
$$[2] \quad R_m = \frac{M_{od}\Delta m(1 - e^{-1})}{t_1 - 0} = 0.632A_b \left( \frac{\rho_p \beta \delta \Delta m}{\tau} \right)$$

where  $\Delta m = (m_0 - m_e)$ ,  $A_b$  is the horizontal area of the fuelbed (square metres),  $\rho_p$  is the dry particle mass density (kilograms per cubic metre),  $\beta$  is the bed packing ratio (cubic metres particles per cubic metre bed), and  $\delta$  is the bed depth (metres). Thus the first-period area drying rate (kilograms per square metre per hour) may be written as

$$[3] \quad R_a = \frac{R_m}{A_b} = 0.632 \left( \frac{\rho_p \beta \delta \Delta m}{\tau} \right) = 0.632 \left( \frac{M_i \Delta m}{\tau} \right) = 0.632 \left[ \frac{\rho_p \Delta m (\sigma M_i / \rho_p)}{\sigma \tau} \right]$$

where the initial fuel load (kilograms per square metre) is  $M_i = \rho_p \beta \delta$ ,  $\sigma$  is the particle surface/volume ratio (metre<sup>-1</sup>),

**Fig. 2.** Sketch of headfire combustion rate  $M_a/\tau_r$  of pine needle beds as a function of fuel-load parameter  $\sigma M_i/\rho_p$ .



and  $\sigma M_i/\rho_p$  is the fuel-load parameter (square metres particle surface area per square metre planar bed area).

**Combustion rate – drying rate similarities**

When a bed of fine fuels is exposed to a source of intense heat, low-temperature volatiles and water initially leave the particles by diffusion, but as particle temperature increases, pyrolysis products and steam exit the particles as a result of a pressure-driven bulk flow; the particles ignite, and a flame eventually develops in the bed (Mardini et al. 1996). For line fires, Nelson (2003) found a relationship between the unit-area burning rate (kilograms per square metre per second) and the fuel-load parameter. This burning rate (hereafter referred to as the combustion rate) is  $M_a/\tau_r$ , where  $M_a$  is the available fuel load (kilograms per square metre), and  $\tau_r$  is the fuelbed reaction (or residence) time (seconds). The fuel-load parameter in eq. 3 also may be written as  $\sigma \beta \delta$  and depends on fuel-particle and fuelbed properties. Figure 2 is a sketch of the results observed when  $M_a/\tau_r$  is plotted against  $\sigma M_i/\rho_p$  for a series of head fires in ponderosa pine needle beds of differing  $M_i$  (Nelson 2003). For lightly loaded beds,  $M_a/\tau_r$  is proportional to  $\sigma M_i/\rho_p$ ; this linear relationship implies constant  $\tau_r$  because  $M_a$  is roughly proportional to  $M_i$  (through combustion efficiency), and  $\sigma$  and  $\rho_p$  are regarded as constants. In this case, beds are porous and air is plentiful, so the combustion rate is proportional to the particle surface area per unit bed planar area (or the fuel load). For heavier beds, the constant combustion rate is independent of loading,  $\tau_r$  is proportional to  $M_a$ , and burning is governed by the air available for combustion (i.e., burning is ventilation controlled).

We test the general applicability of these combustion-rate relationships to the drying of longleaf pine needle beds by assuming that area rates of water loss (kilograms per square metre per second) due to evaporation and diffusion also are a function of the fuel-load parameter (the area drying rate is in hours rather than seconds because of differences in time scale). In the analysis of results section, we describe the attenuation (or delay) of vapor transfer to the atmosphere due

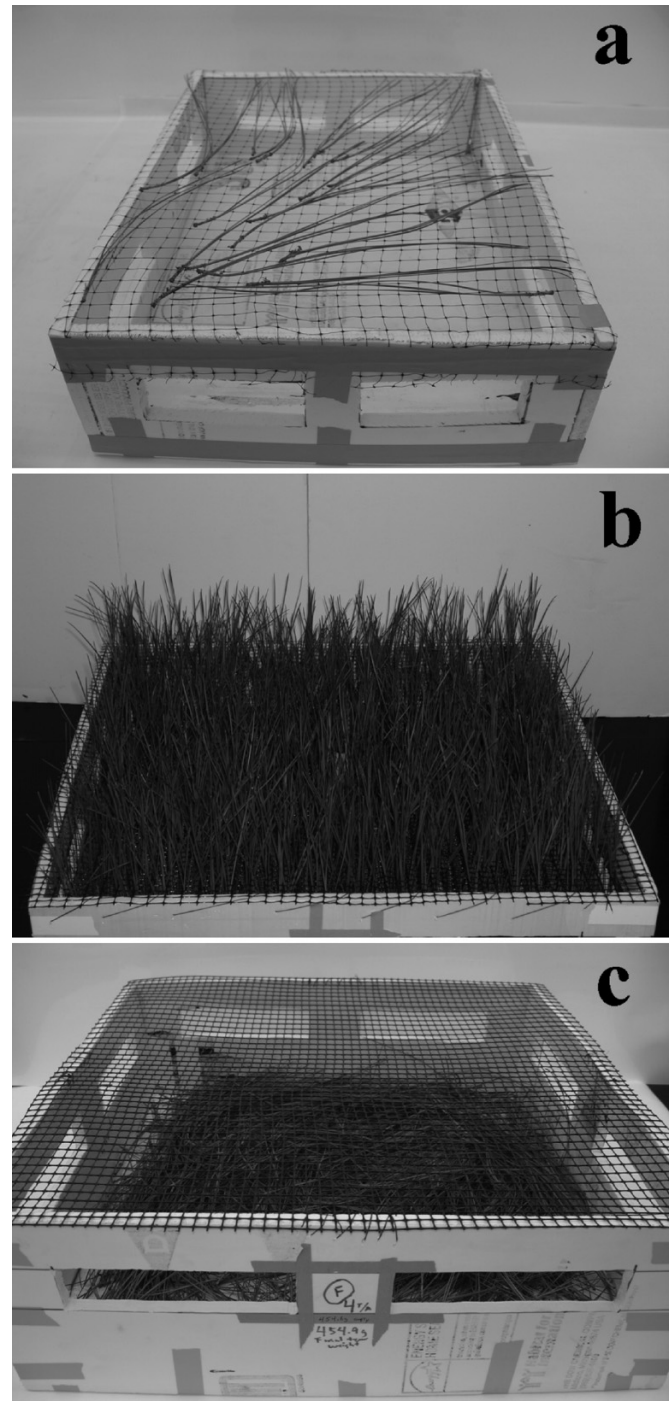
to the presence of needles in terms of the fuelbed radiative absorption coefficient (Vaz et al. 2004).

## Methods

The study was conducted in the laboratory facilities of the Joseph W. Jones Ecological Research Center, a 115 km<sup>2</sup> privately owned research reserve in Baker County, Georgia, USA. Recently, fallen longleaf pine litter was collected from a 19-year-old longleaf pine plantation that had not received fertilizer amendments or chemical treatments. Needles were collected in December 2006 and May 2007 for use in drying experiments conducted in January and June 2007, respectively. The needles collected in late May were recently abscised as a result of the severe spring drought of March–May 2007 (Florida Division of Forestry 2007). Intact nonweathered needles were sorted to eliminate broken or discolored needles and then separated into 200 bundles of an estimated 50 g dry biomass each to facilitate construction of fuelbeds with the desired loadings. For each set of experiments, we achieved consistent initial moisture content by submerging the bundles in water inside a plastic storage bin so that all needles were uniformly moistened; the bin was inside a high-humidity walk-in conditioning cabinet. In January, the needles reached a moisture content fraction near unity after 48 h; for the June experiment, however, the relatively dry needles required more than 5 days of submersion to achieve a moisture content fraction approximating that for January. For 12 h following soaking, excess surface water was removed by storing the bundles vertically within a closed bin in the cabinet. Fuelbeds then were constructed inside the high-humidity cooler to minimize moisture loss (~10 min); after construction, the beds were quickly transported to the drying laboratory where weighing was begun immediately.

The experimental design includes two blocks, January and June, for which the external drying conditions differed. Within blocks, needle loadings of 0.224, 0.448, and 0.896 kg·m<sup>-2</sup> (1, 2, and 4 tons/acre) were used at needle angles of 0° and 90°, measured from horizontal. Vertical needles represented particles standing in clumps of grass or hanging from aerial fuels; the flat needles were arranged to mimic distribution on the forest floor. We included drying runs for needles tilted at approximately 45° in the January experiment, but the results were statistically indistinguishable from those of the 90° treatments (*t*-test results), and thus the data of the 45° treatments were subsequently included with those of the 90° treatments for the statistical analysis in this study. For purposes of reference, beds of individual particles in a flat orientation (mean loading = 0.044 kg·m<sup>-2</sup> (0.2 ton/acre)) were included in the January and June experiments, and a 0.112 kg·m<sup>-2</sup> (0.5 ton/acre) treatment also was added in June to improve regression analyses. The vertical needles were supported with foam board trays with layers of plastic netting along the top and bottom of each tray to keep the needles tilted at 45° or 90°. In the beds of flat needles, particles were arranged randomly on the bottom surface of the tray (no plastic netting). The horizontal area of the beds of vertical and flat needles was 0.37 m<sup>2</sup>. For data on individual particles, 21 needles were carefully placed on the top netting of the tray (area =

**Fig. 3.** Longleaf pine needle beds during drying with needles arranged as (a) individual needles loaded at 0.044 kg·m<sup>-2</sup> (0.2 ton/acre), (b) vertical needles at 0.896 kg·m<sup>-2</sup> (4 tons/acre), (c) flat needles at 0.896 kg·m<sup>-2</sup> (4 tons/acre).



0.14 m<sup>2</sup>) so that they were separated by at least 0.5 cm. Because the entire surface of each needle was fully exposed to ambient air, we assume that the observed first-period time-lags and area drying rates for individual particles apply to both vertically and horizontally oriented needles (i.e., that any differences were within the error of measurement and primarily caused by differences in drying conditions). Figure 3 shows trays containing individual, vertical, and flat nee-

**Table 1.** Fuelbed characteristics for January and June 2007 experiments on drying of longleaf pine (*Pinus palustris*) needles.

Needle angle (°)	$M_{od}$ (kg)	$M_i$ (kg·m <sup>-2</sup> )	$\beta$	$\delta$ (m)	$m_0$
<b>January</b>					
Indiv. particles	0.006	0.041	0.0200	0.004	1.26
90	0.090	0.241	0.0015	0.325	1.08
90	0.172	0.462	0.0027	0.335	1.07
90	0.337	0.906	0.0050	0.355	1.12
45	0.078	0.209	0.0014	0.300	1.08
45	0.169	0.453	0.0031	0.290	1.13
45	0.331	0.889	0.0057	0.305	1.08
0	0.088	0.235	0.0180	0.026	1.12
0	0.170	0.456	0.0260	0.034	1.11
0	0.332	0.892	0.043	0.041	1.13
<b>June</b>					
Indiv. particles	0.006	0.046	0.0230	0.004	1.32
90	0.048	0.130	0.0008	0.330	1.17
90	0.135	0.364	0.0021	0.335	1.08
90*	0.098	0.263	0.0016	0.325	1.00
90	0.200	0.537	0.0031	0.345	1.06
90	0.387	1.040	0.0057	0.360	1.12
0	0.048	0.130	0.028	0.009	1.04
0	0.097	0.261	0.021	0.024	1.19
0	0.186	0.500	0.031	0.032	1.16
0	0.397	1.066	0.047	0.045	1.12

**Note:**  $M_{od}$ , oven-dry mass;  $M_i$ , fuel load;  $\beta$ , packing ratio;  $\delta$ , bed depth;  $m_0$ , initial moisture content. January mean temperature and relative humidity were 21.1 °C and 31%, resulting in  $m_e = 0.095$ ; June mean temperature and relative humidity were 21.1 °C and 61%, resulting in  $m_e = 0.15$ . Fuelbed area = 0.37 m<sup>2</sup>; for individual particles, area = 0.14 m<sup>2</sup>. Particle surface/volume ratio = 6071 m<sup>-1</sup>; particle mass density = 508 kg·m<sup>-3</sup> (Hough and Albini 1978). The January individual particle bed depth  $\delta = 0.004$  m was not measured; it is assumed to be equal to the corresponding value for June.

\*This bed is a repeat of the previous bed to achieve a loading closer to the target value  $M_i = 0.224$  kg·m<sup>-2</sup> (1 ton/acre); it nevertheless provides a valuable data point for regression analyses.

dles. Figure 3b shows that the upper half of the heavily loaded bed of vertical needles ( $M_i = 0.896$  kg·m<sup>-2</sup> (4 tons/acre)) involves meshing of needles in proximity or in contact with each other — primarily because of drying stresses and the effects of gravity. In this figure, the needle mass in the lower half of the bed apparently retains its original configuration, whereas the bending of needles in the upper half of the bed causes bed shrinkage and increased fuel continuity. These two factors may lead to increased resistance to vapor flow; this resistance is hereafter considered to be due to a fuelbed bulk density gradient. Windows in the four sides of all trays aided the simulation of drying in open air and facilitated bed construction and removal of needles after each drying run. At times during the individual particle tests, needles in a single fascicle separated because of drying stresses and came into contact with adjacent needles. Thus when possible, needles were rearranged slightly to maintain spacing. A factor ignored in these experiments was the effect of cuticle thickness differences on timelags and drying rates; we assume that any effects so introduced were between blocks, rather than within them. Pertinent fuelbed characteristics are presented in Table 1.

After the needles had soaked and drained and beds were

constructed, the mean initial moisture fractions,  $m_0$ , within the January and June experimental blocks were 1.12 and 1.13, respectively. Fuelbeds in both blocks were weighed for 3.5 days following construction or until moisture loss was <0.02 g per sampling interval. The lightly loaded beds approached equilibrium with the ambient air, but mass readings for the heavier beds were stopped prior to equilibrium. Thus we do not have data to confirm that any of the beds achieved true equilibrium. The most important difference between the January and June experiments was in laboratory relative humidity (RH) — 31% and 61% for January and June, respectively. The mean value of laboratory temperature for both blocks was 21.1 °C (70 °F). Temperature and RH remained relatively constant in the drying laboratory for the entire period, with no more than a 10% fluctuation in either variable during each set of experiments. The procedure for computing equilibrium moisture content fraction,  $m_e$ , at laboratory conditions was to estimate  $m_e$  for a given RH from the 26.7 °C (80 °F) desorption isotherm for longleaf pine needles presented in fig. 3 of Blackmarr (1971) and apply the temperature correction in eq. 2B of Anderson et al. (1978). This procedure gives  $m_e$  values of 0.095 and 0.15 for the tests in January and June, respectively. The drying data were analyzed by computing moisture content fraction,  $E$ , from eq. 1 and listing the  $E$  values and corresponding drying times in a spreadsheet. We then determined the first-period timelag,  $\tau$ , from the time corresponding to  $E = 0.368$  using interpolation.

The overall experiment was a completely randomized unbalanced block design analyzed using ANOVA with needle loading and needle angle as fixed effects in PROC MIXED (SAS Institute Inc. 2003). Blocks were defined as January and June sampling periods. Simple-effect slices of loading by angle interactions were used to examine differences at each level of fuel load. We studied timelag,  $\tau$ ; area drying rate,  $R_a$ ; and fraction of evaporable water content,  $E$ , with both linear and nonlinear regressions performed using SigmaPlot/SigmaStat (SigmaPlot 1997). Nonlinear regressions were calculated iteratively with a maximum likelihood best-fit curve. Goodness of fit between linear and curvilinear regressions was determined based on coefficients of variation and statistical significance.

## Results

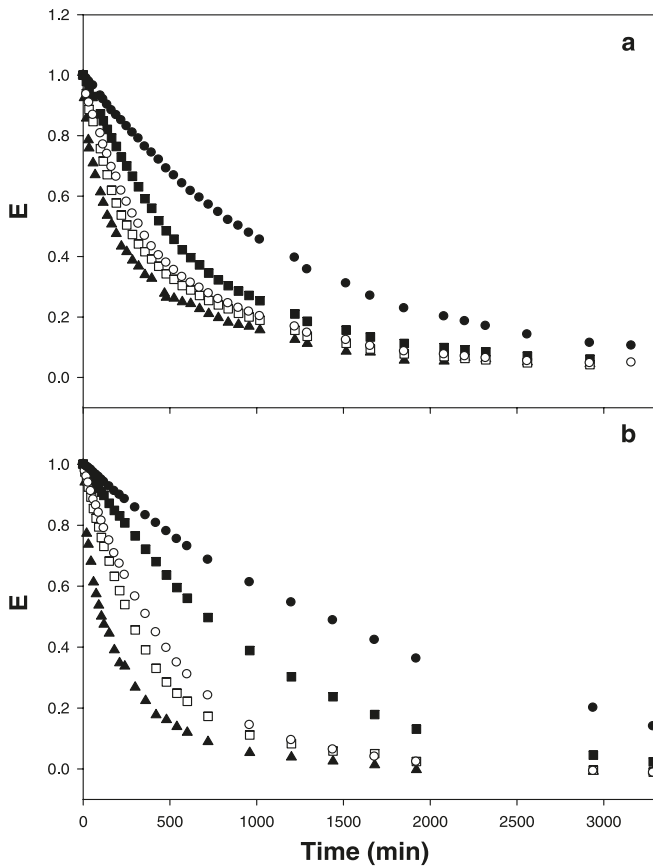
Both fuelbed loading and needle arrangement significantly altered first-period timelags in beds of longleaf pine needles ( $P < 0.0005$ ; Table 2). Needle arrangement (horizontal versus vertical) also significantly interacted with fuel load ( $P < 0.006$ ; Table 2), dramatically lengthening first-period timelags in horizontal needle beds, while causing only modest linear increases in drying rates of vertical needles. Timelags of beds composed of vertically oriented needles (4.4 to 8.6 h) more closely approximated those of individual particles (3.3 to 5.3 h) and were modestly influenced by fuel loading. Beds of horizontally arranged needles dried with timelags from 6.5 to 31.6 h.

This interaction between fuel load and needle arrangement is illustrated in the drying curves in Fig. 4. For both experimental blocks (January and June), decay curves of the evaporable water fraction,  $E$ , versus time,  $t$ , for each run in-

**Table 2.** Mixed-model results for randomized block design with first-period timelag comparison by loading and angle treatments (SAS Institute Inc. 2003); type 3 tests of fixed effects of needle loading and angle on timelags are presented.

Effect	Num. df	Denom. df	F	P > F
Loading	3	9.44	16.34	0.0004
Angle	1	9.08	29.39	0.0004
Loading × angle	3	9.03	8.3	0.0058

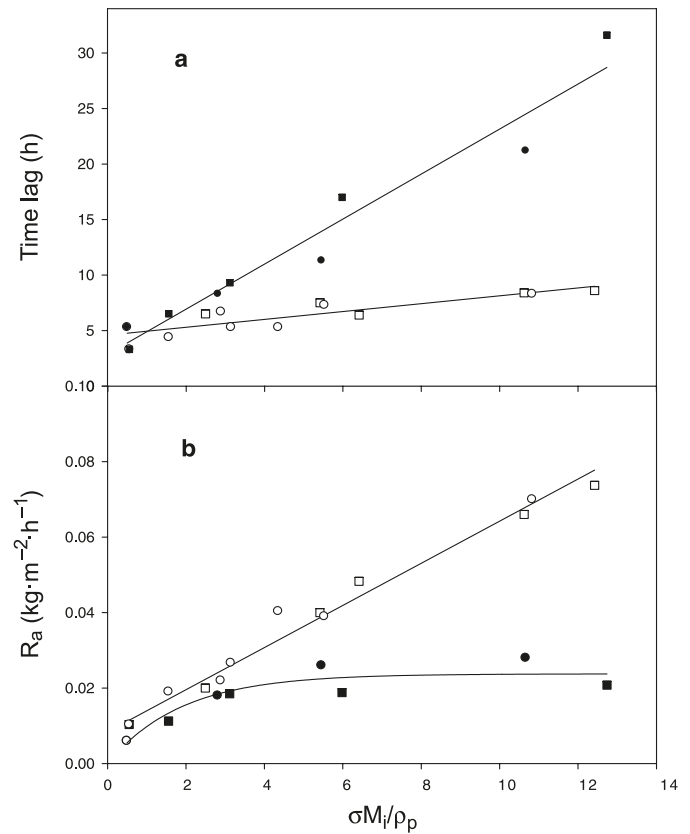
**Fig. 4.** Longleaf pine needle drying curves of unaveraged evaporable water fraction,  $E$ , versus time,  $t$ , for experimental blocks in January and June 2007: (a) January, (b) June. Closed triangles, individual needles; squares, 0.448 kg·m<sup>-2</sup> (2 tons/acre); circles, 0.896 kg·m<sup>-2</sup> (4 tons/acre); open symbols, vertical needles; closed symbols, flat needles.



indicate the magnitude of separation for the runs shown, with individual particles drying at the fastest rate in each case, and the more heavily loaded beds drying at the slowest rates.

Figure 5 shows plots of the first-period timelag,  $\tau$ , and area drying rate,  $R_a$ , versus fuel-load parameter,  $\sigma M_i/\rho_p$ , for the January and June drying runs; these data are summarized in Table 3. In Fig. 5a,  $\tau$  is plotted versus  $\sigma M_i/\rho_p$  for the two data sets. The data do not extrapolate to the origin because particle timelag,  $\tau_p$ , always exceeds zero; thus the beds of individual needles provide reference data for  $\tau$  and  $\sigma M_i/\rho_p$  in the present experiments. Small differences in slope (between blocks) are evident for the vertical needles; the flat needles exhibit larger differences. For the flat needles,

**Fig. 5.** First-period timelag,  $\tau$ , and area drying rate,  $R_a$ , for drying of longleaf pine needle beds in January and June 2007 as functions of the fuel-loading parameter,  $\sigma M_i/\rho_p$ : (a)  $\tau$ , (b)  $R_a$ . Circles, January; squares, June; open symbols, vertical needles; closed symbols, flat needles.



slopes of the June data exceed those for January data by a factor of about 1.5. Nelson (1969) shows that  $\tau$  for sawdust beds and wooden square rods ( $m_0 \sim 0.93$ ) is proportional to  $[100/(100 - RH)]$ . If this relationship is applied to the flat needle data of Fig. 5a, then  $\tau$  for June exceeds that for January by a factor of 1.8, supporting the notion that the difference in slopes is due to differences in laboratory RH.

The linear relationship between  $\tau$  and  $\sigma M_i/\rho_p$  for the flat needles in Fig. 5a suggests that a single drying regime determined the magnitude of  $\tau$ . For these needles,  $\tau$  varies from 6.5 to 31.6 h, whereas for the vertical needles  $\tau$  ranges only from 4.4 to 8.6 h. The June data for vertical needles suggest that for  $\sigma M_i/\rho_p < 4.4$ ,  $\tau$  is constant at about 5 h, whereas behavior of the corresponding January data is unclear because there are only two data points. The vertical needles may have approached a drying regime in which moisture loss is controlled by the particles ( $\tau = \tau_p = \text{constant}$ ), but the drying of these needles was compromised in a minor way because of bed bulk density gradients. The increase in bulk density in the upper half of these beds (Fig. 3b) may have caused a reduction in the rate of vapor diffusion — an effect that should become more pronounced as fuel loading increases.

In Fig. 5b,  $R_a$  is plotted against  $\sigma M_i/\rho_p$  for the January and June experiments. In the case of heavily loaded beds of vertical needles,  $R_a$  can be up to 3.5 times greater than that for flat needles of comparable loading, whereas the lightly

**Table 3.** First-period timelags, area drying rates, and fuelbed parameters for January and June 2007 experiments on drying of longleaf pine (*Pinus palustris*) needles.

Needle angle (°)	$\tau$ (h)	$R_a$ (kg·m <sup>-2</sup> ·h <sup>-1</sup> )	$\sigma M_i/\rho_p$	$l_t$ (m)	$\delta/l_t$	$m_0 - m_e$
<b>January</b>						
Indiv. particles	5.3	0.006	0.49	0.03	0.13	1.17
90	6.7	0.022	2.89	0.44	0.74	0.98
90	7.3	0.039	5.53	0.24	1.40	0.97
90	8.3	0.070	10.83	0.13	2.73	1.02
45	6.5	0.020	2.49	0.47	0.64	0.98
45	7.5	0.040	5.42	0.21	1.38	1.04
45	8.4	0.066	10.62	0.12	2.54	0.98
0	8.3	0.018	2.81	0.04	0.65	1.02
0	11.3	0.026	5.46	0.03	1.13	1.01
0	21.2	0.028	10.66	0.02	2.05	1.04
<b>June</b>						
Indiv. particles	3.3	0.010	0.55	0.04	0.10	1.17
90	4.4	0.019	1.56	0.85	0.39	1.02
90	5.3	0.040	4.35	0.31	1.08	0.93
90*	5.3	0.027	3.15	0.41	0.79	0.85
90	6.4	0.048	6.41	0.22	1.57	0.91
90	8.6	0.074	12.42	0.12	3.00	0.97
0	6.5	0.011	1.56	0.02	0.45	0.89
0	9.3	0.018	3.12	0.03	0.80	1.04
0	17.0	0.019	5.98	0.02	1.60	1.01
0	31.6	0.021	12.74	0.01	4.50	0.97

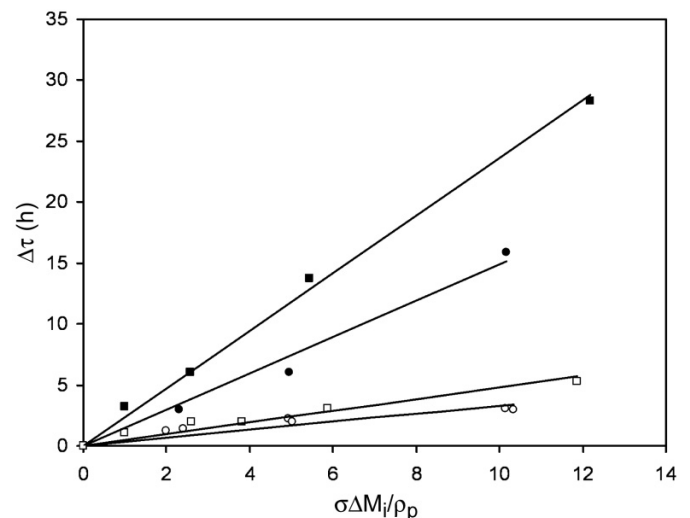
**Note:**  $\tau$ , timelag;  $R_a$ , area drying rate;  $\sigma M_i/\rho_p$ , fuel-load parameter;  $l_t$ , transport mean free path;  $\delta/l_t$ , bed depth to mean free path ratio; ( $m_0 - m_e$ ), evaporable moisture content. Particle surface/volume ratio = 6071 m<sup>-1</sup>; particle mass density = 508 kg·m<sup>-3</sup> (Hough and Albini 1978).  
 \*This bed is a repeat of the previous bed to achieve a loading closer to the target value  $M_i = 0.224$  kg·m<sup>-2</sup> (1 ton/acre); it nevertheless provides a valuable data point for regression analyses.

loaded beds for both vertical and flat needles tend to be independent of needle orientation. Linearity of  $R_a$  for the vertical needles over most of the range in  $\sigma M_i/\rho_p$  (a small decrease in  $R_a$  is apparent for  $\sigma M_i/\rho_p > 10$  because of bulk density gradients) indicates that they dried in the particle surface area controlled regime (Fig. 2). A similar interpretation applies to the first few data points for the flat needles, which display a slope roughly parallel to that of the vertical needles for  $\sigma M_i/\rho_p < 4$ . The flat needle data also suggest that  $R_a$  is independent of fuel load when  $\sigma M_i/\rho_p > 4$  (Fig. 2). The smaller values of  $R_a$  for June are due to larger  $\tau$  values in the denominator of eq. 3 for  $R_a$  (Table 3). Furthermore, the transition to zero slope occurs in the neighborhood of  $\sigma M_i/\rho_p = 4$ . In the next section, we show that these results for the flat needles are consistent with the interception, adsorption, and subsequent desorption of vapor molecules owing to the fuelbed radiative absorption coefficient (Steward 1974; Vaz et al. 2004).

**Analysis of results**

Data in Fig. 5a suggest a tendency for first-period timelags of the vertical needles to approach the ideal condition  $\tau = \tau_p = \text{constant}$ . Such a result would indicate a zero effect of loading on fuelbed timelags. This ideal condition can be only approximated because the relative humidity of air around an embedded needle in all likelihood exceeds that around a single isolated needle when ambient conditions are the same. The drying characteristics of the single needle re-

**Fig. 6.** First-period timelag difference  $\Delta\tau$  ( $= \tau - \tau_p$ ) versus dimensionless fuelbed loading difference  $\sigma\Delta M_i/\rho_p$  ( $\Delta M_i = M_i - M_{ip}$ ) for drying of longleaf pine needle beds in January and June 2007. Timelag and bed loading for individual particles are  $\tau_p$  and  $M_{ip}$ , respectively. Circles, January; squares, June; open symbols, vertical needles; closed symbols, flat needles.



flect the effects of fuel particle physical and chemical properties on the fuelbed timelag, but do not account for gradients in temperature and relative humidity, the effects of which must be clarified with theories of evaporation and

**Table 4.** First-period timelag difference,  $\Delta\tau$ , as a function of the dimensionless fuelbed loading difference,  $\sigma(M_i - M_{ip})/\rho_p$ , or fuel-load parameter,  $\sigma M_i/\rho_p$  (eq. 5 or 6).

Treatment	RTO		OLS		
	<i>S</i>	<i>R</i> <sup>2</sup>	<i>b</i>	<i>S</i> '	<i>R</i> <sup>2</sup>
<b>January</b>					
Horizontal	1.487	0.981	-0.612	1.567	0.986
Vertical	0.331	0.811	0.548	0.260	0.916
<b>June</b>					
Horizontal	2.359	0.997	0.470	2.306	0.998
Vertical	0.481	0.926	0.504	0.417	0.969

**Note:** Parameters are shown for regression through the origin (RTO) and ordinary least squares (OLS) for the January and June 2007 timelag data.

diffusion. We propose that timelag  $\tau$  consists of two parts: (1)  $\tau_p$  due to fuel particle characteristics, and (2)  $\Delta\tau = \tau - \tau_p$  due to the influence of fuel loading. Both parts are affected by the external drying conditions. Thus  $\tau$  is given by

$$[4] \quad \tau = \tau_p + \Delta\tau$$

In the present experiments,  $\tau_p$  was measured by repeatedly weighing a bed of widely spaced needles whose loading is designated as  $M_{ip}$ . Thus a modified fuel-load parameter may be written as  $\sigma\Delta M_i/\rho_p$ , where  $\Delta M_i = (M_i - M_{ip})$ . A plot of  $\Delta\tau$  versus  $\sigma\Delta M_i/\rho_p$  ensures that the experimental data pass through the origin if they are truly linear; Fig. 6 shows such a plot for the January and June data. Both the figure and the linear regression show that most of the variability in  $\Delta\tau$  is explained by  $\Delta M_i$ . In presenting the data in this form, we assume that for the external drying conditions of our experiments  $\Delta\tau$  always equals or exceeds zero. Furthermore, for a different experiment in identical conditions during which individual needles dry in a bed with an  $M_{ip}$  that is smaller than that of the present experiments, we expect the measured  $\tau_p$  will (neglecting measurement error) equal that of the present experiments. In Fig. 6, least squares regression lines (forced through the origin) are constructed according to the equation

$$[5] \quad \Delta\tau = \tau - \tau_p = \frac{S\sigma(M_i - M_{ip})}{\rho_p}$$

with regression results presented in Table 4. For comparison, Table 4 also displays regression parameters for an ordinary least squares analysis according to

$$[6] \quad \Delta\tau = \tau - \tau_p = b + S' \left( \frac{\sigma M_i}{\rho_p} \right)$$

where  $b$  and  $S'$  are the intercept and slope, respectively, of the ordinary regression lines (not shown in Fig. 6). In Table 4, slope  $S'$  differs only slightly from slope  $S$  of eq. 5; coefficients of determination ( $R^2$ ) are slightly larger for the ordinary analysis. Substitution of eq. 5 into eq. 3 and use of data in Table 4 lead to a predictive expression for area drying rate  $R_a$  given by

$$[7] \quad R_a = 0.632 \left[ \frac{\rho_p \Delta m(\sigma M_i/\rho_p)}{\sigma\tau} \right] = \frac{0.053\Delta m(\sigma M_i/\rho_p)}{\tau_p + S\sigma(M_i - M_{ip})/\rho_p}$$

where  $\rho_p/\sigma = 508/6071 = 0.0837 \text{ kg}\cdot\text{m}^{-2}$  (Hough and Albin 1978). From eq. 6,

$$[8] \quad R_a = \frac{0.053\Delta m(\sigma M_i/\rho_p)}{\tau_p + b + S'(\sigma M_i/\rho_p)}$$

**Radiative absorption coefficient and fuelbed drying**

Here we describe how the fuelbed radiative absorption coefficient can affect the drying of natural or manually constructed pine needle beds. Steward (1974) discusses the radiative absorption coefficient of a bed of fuel particles and lists three assumptions: (1) the particles are uniformly distributed throughout the fuelbed depth, (2) the particles are black, so that all radiation incident on them is absorbed, (3) radiative wavelengths are small compared with the particle diameter. Under these conditions, the absorption coefficient  $k$  (square metres of particle surface per cubic metre of bed volume) is independent of the wavelength and given by

$$[9] \quad k = \frac{\sigma\beta}{4}$$

where the 1/4 multiplier of  $\sigma\beta$  accounts for the fractional surface area of a single particle exposed to radiation. Units of  $k$  are reciprocal length, so  $1/k$  may be regarded as an estimate of the transport mean free path,  $l_t$ , of radiation in the bed (Modest 1993). We apply these concepts to vapor diffusion within a fuelbed by assuming that  $l_t$  is the mean distance traveled by vapor molecules before being reabsorbed by fuel particles. Thus  $l_t$  exceeds the molecular mean free path of water vapor at room temperature and atmospheric pressure ( $\sim 4.2 \times 10^{-8} \text{ m}$ ) by several orders of magnitude. The transport mean free path is

$$[10] \quad l_t = \frac{1}{k} = \frac{4}{\sigma\beta}$$

where  $l_t$  ranges from about 0.01 to 0.85 m in the present experiments. Similarly, the bed depth to mean free path ratio,  $\delta/l_t$ , ranges from about 0.1 to 4.5 (Table 3).

For a given fuel type, the effects of fuelbed loading on the first-period timelag can be expressed in terms of the  $\delta/l_t$  ratio. One way of doing this is to use eqs. 6 and 10 to write timelag  $\tau$  as

$$[11] \quad \tau = \tau_p + b + S' \left( \frac{\sigma M_i}{\rho_p} \right) = \tau_p + b + 4S' \left( \frac{\sigma\beta\delta}{4} \right) = \tau_p + b + 4S' \left( \frac{\delta}{l_t} \right)$$

where slope  $S'$  is related to particle orientation. Equations 11 may be used with the OLS results in Table 4 to develop  $\tau$  equations for beds of flat and vertical needles within blocks (a similar analysis could be done using eq. 5).

Table 4 shows that  $S'$  for the vertical needles is about six times smaller than for the flat needles; we speculate that  $S'$  for the vertical needles tends toward zero, and that the observed nonzero values are due to fuelbed bulk density gra-

dients. Hypothetically, if there had been no such gradients (i.e., perfectly vertical needles), we would have observed  $S' = 0$  and  $\tau = \tau_p = \text{constant}$ . In the present experiments, however,  $S' > 0$  and drying of the vertical needles apparently takes place with small, but significant, interception of vapor molecules by particles in the bed (especially for the heavier loadings);  $\tau$  only approaches  $\tau_p$ . In eq. 11,  $(\tau_p + b)$  exceeds  $S'(\sigma M_i/\rho_p)$  by a factor of 2 or more, so the denominator is roughly constant and leads to a linear relationship (though weak) between  $\tau$  and  $\sigma M_i/\rho_p$  (Fig. 5a). Timelag,  $\tau$ , is determined by the rate of water loss from the particles because free (or slightly hindered) vapor diffusion in air is greater than moisture diffusion in pine needles. Thus drying takes place in a particle-controlled regime for the beds of vertical needles.

For beds of flat needles, the larger  $S'$  values (by a factor of 6) result in  $\tau$  values that are about 1.5 to 3.5 times greater than those for the vertical needles (Table 3). The effect of loading on the magnitude of  $\tau$  clearly is much stronger than for the vertical needles. We believe the mechanism causing this larger  $\tau$  (or diffusion delay) is similar to the attenuation of a radiant beam by the bed; many of the vapor molecules diffusing toward the ambient air are repeatedly intercepted by needles prior to escaping the bed. We set  $\delta/l_t \sim 1$  as a lower limit on the bed depth to mean free path ratio for drying of the heavier beds of flat needles. Apparently, the significantly delayed vapor diffusion rate drops below the particle diffusion rate, inducing a bed-controlled drying regime. Thus timelag  $\tau$  is determined by the structure of the bed (i.e., by the radiative absorption coefficient). Exceptions to this behavior occur in lightly loaded flat-needle beds ( $0.112$  and  $0.224 \text{ kg}\cdot\text{m}^{-2}$ ) for which  $l_t > \delta$  and drying takes place in the particle-controlled regime; nevertheless, a change in mechanism is not evident in the data of Fig. 5a.

The arguments above concerning the effect of loading on the timelag can be used to interpret the area drying rate,  $R_a$ , versus  $\sigma M_i/\rho_p$  data in Fig. 5b. For the vertical needles, the slightly hindered rate of vapor diffusion in bed air spaces is large relative to the rate of diffusion in the particles. Because  $(\tau_p + b)$  is constant and exceeds the remaining term in the denominator of eq. 8 by at least a factor of 2,  $R_a$  is roughly proportional to  $\sigma M_i/\rho_p$  for a series of runs in which  $\Delta m$  is approximately constant. This result is observed in Fig. 5b for all beds of vertical needles. We note also that  $R_a$  is proportional to  $M_w/\tau$ , where  $M_w = M_i \Delta m$  = the available water (i.e., the total water available for loss from unit area of the fuelbed by evaporation and (or) diffusion). Thus  $M_w$  is a direct analogue of the available fuel loading,  $M_a$  (the unit area fuelbed mass loss due primarily to volatilization of original fuel) — a variable critical to understanding fire behavior.

For the heavier beds of flat needles, we have assumed that  $\delta > l_t$  and that vapor diffusion in the bed is slowed because of adsorption of vapor molecules by intervening particles and subsequent desorption. As previously discussed, we expect  $\delta < l_t$  when fuel loads are sufficiently small and the flat needles dry like vertical needles (i.e., by particle-controlled drying). Except for these lightly loaded beds, the term  $S'(\sigma M_i/\rho_p)$  in eq. 8 exceeds  $(\tau_p + b)$  by a factor of 2 or more, so the denominator is effectively proportional to the fuel-load parameter. Thus this parameter divides out of eq. 8, and  $R_a$  is essentially constant within blocks — in

agreement with Fig. 5b. For these heavily loaded beds, drying rates are controlled by the obstruction of vapor diffusion as a result of interception, adsorption, and later desorption of vapor molecules rather than by the particle surface area (or fuel loading).

We have proposed  $\delta/l_t \sim 1$  as the criterion for which values exceeding unity indicate that the drying of flat-needle beds is regulated by the radiative absorption coefficient. This criterion may be used to estimate the value of  $\sigma M_i/\rho_p$  at which the transition from particle-controlled to bed-controlled drying occurs. Combining the criterion with eq. 11 leads to  $\delta/l_t = \sigma M_i/4\rho_p = 1$  and

$$[12] \quad (\sigma M_i/\rho_p)_t = 4$$

where subscript t indicates the transition value. Inspection of Fig. 5b indicates a transition in  $R_a$  for the flat needles in approximate agreement with eq. 12. The ratio  $\sigma/\rho_p$  is 11.95; thus for the present experiments, the transition from particle-controlled to bed-controlled drying occurs at about  $M_i = 0.33 \text{ kg}\cdot\text{m}^{-2}$ .

We caution the reader that the approximations in the above discussion of eqs. 8 to 12 indicate only causal relationships between the radiative absorption coefficient and effects of fuelbed loading on  $\tau$  and  $R_a$ . They show that these relationships are consistent with the experimental data in Fig. 5. One may obtain calculated values of  $\tau$  and  $R_a$  in excellent agreement with the data by using eqs. 6 and 8 in conjunction with Table 4.

## Discussion

Anderson (1990) reports a wide range of response times for common fine fuels in western forests; on the other hand, this study illustrates the dramatic effects of fuelbed properties — loading and arrangement — on first-period timelags likely to occur in longleaf pine litter. The loading treatments of this study represent the range of conditions commonly found in longleaf pine woodlands (Ottmar et al. 2003), with an increase in loads leading to an increase in timelags across all angle treatments. Tests of needle angle effects within blocks showed timelag differences between vertically and horizontally oriented fuels, but not between angles of needles ( $45^\circ$  vs.  $90^\circ$ ).

The wide range of timelags among treatments illustrates the importance of understanding fuelbed properties such as initial loading and their potential to dramatically affect expected fire behavior through modifications in wetting and drying rates. For vertical fuels, the first-period timelag is weakly dependent on fuelbed loading, whereas in beds of flat needles, the timelag depends strongly on fuel load.

The drying of wet pine needle beds generally occurs in two phases. First, there is evaporation of free water on the particle surface followed by movement of internal liquid water and then bound water to the surface and subsequent evaporation into bed air spaces. Second, there is movement of vapor molecules toward the ambient air along a highly tortuous path as a result of evaporation from cylindrical needles, molecular collisions, interception by particles, and subsequent desorption, all of which produce vapor movement in multiple directions. Despite the repeated occurrence of these events, there is a general upward movement of

water vapor toward the ambient air because of the gradient in vapor pressure that exists owing to the relative humidity difference between the bottom of the bed and the ambient air. For the vertical needles and lightly loaded flat needles, the resistance to vapor flow is small, so the area drying rate is limited by the rate at which water can evaporate from the needles. This rate is proportional to the needle surface area (or fuelbed loading). On the other hand, the heavily loaded flat needles constitute a relatively large barrier to vapor flow. The rate at which water evaporates from the needles apparently exceeds the rate of hindered vapor diffusion, so the bed drying rate is independent of fuelbed loading and controlled by structure of the bed (i.e., by the extent to which the bed can accommodate vapor diffusion despite interference from needles).

Area drying rates for beds composed of vertical needles differ greatly from those for the flat-needle beds. In their discussion of the passage of radiant beams through pine needle beds, Vaz et al. (2004) show experimentally that the multiplier of  $1/4$  in eq. 9 is approximately correct for natural pine needle beds, but do not present experimental values of the multiplier for radiative transfer within a bed of vertically oriented needles. The results in Fig. 5b suggest that a value of  $\sigma M_i/\rho_p \gg 4$  would be required to describe attenuation of radiant beams passing through such beds. Alternatively, a bed-controlled drying regime may never occur in pine needle beds in which the particles are vertically oriented.

Our analogy between radiative transfer and directional diffusion of water vapor through a pine needle bed is based on similarities between a beam of photons emitted from a radiation source at the base of the bed and the stream of water vapor molecules that moves toward the ambient air. The attenuation of radiation in needle beds with variable particle properties has been treated in detail by Vaz et al. (2004). For the present paper, major points of similarity are (1) transfer of both photons and vapor molecules is by diffusion, (2) photons and vapor molecules are absorbed and scattered by intervening needles in their vertical paths of travel, (3) emitted radiation travels in straight lines until it is absorbed or scattered by particles, whereas the exit of water vapor from needles also is multidirectional and yet produces a net upward movement within the bed owing to the gradient in vapor pressure. Though imperfect at the molecular level, this analogy suggests that the concentration of vapor is reduced as the vapor diffuses upward in the same way that the intensity of a beam of radiation is reduced as it travels through a fuelbed. For both processes the reduction apparently is governed by the fuelbed extinction coefficient associated with Beer's law of radiation attenuation by an absorbing-scattering medium (Steward 1974). By assuming that fuel particles such as pine needles are radiatively black, Steward (1974) and Vaz et al. (2004) treat the radiative scattering coefficient of the beds as zero. The same assumption is made in this paper.

## Applications

The results of this study should be useful in the research and operational arenas within forest fire management. In the former case, they can guide follow-on studies to provide a more complete understanding of moisture timelag and area

drying rate in a variety of fuel types. A question that follows from the present study (conducted at initial fuel moisture fractions of about unity) is the following: Would results generally similar to those found in the current study be observed when initial moisture contents are near to or below the point of fiber saturation ( $\approx 0.3$ )? The results of Anderson's (1990) comprehensive research suggest the answer will be yes. Thus the present study should be repeated at moisture fraction levels below 0.3 and possibly extended to cover two or three timelag periods rather than only one. Similarly, adsorption measurements over a large range of initial moisture contents would provide a more complete understanding of sorption processes in forest fuels when ambient conditions are constant. Conditions are rarely constant in the forest, however, and research is needed to incorporate fuelbed properties into the problem of diurnal moisture content prediction where possible. As a simple example, time-lags from sorption studies like the present one can be inserted into a suitable solution of the diffusion equation and combined with pertinent weather data to develop a simple model for predicting diurnal fuel moisture content fraction in the range below 0.3. More comprehensive diurnal models should make use of the moisture diffusivity — a variable inversely related to the timelag.

Fine-fuel moisture is a determinant of fire behavior and a critical input to fire spread models and systems of fire behavior prediction (Andrews et al. 2005; Rothermel 1972) and other systems as well. Our finding that two drying regimes occur in longleaf needle beds when  $\sigma M_i/\rho_p$  is about 4 provides indirect support of the standard value  $1/4$  as a multiplier of  $\sigma\beta$  in eq. 9 for the fuelbed radiative absorption coefficient. Further investigation is needed of the significance of  $\sigma M_i/\rho_p = 4$  as a criterion for identifying two regimes of fuelbed drying (Fig. 5b) and fuelbed combustion (Fig. 2). If the  $\sigma M_i/\rho_p = 4$  criterion is corroborated in future studies of combustion and moisture exchange, then researchers and land managers can use it to generate fuels and fire behavior systems that identify specific regimes of fuel moisture change and combustion behavior. Along these lines, modeling tools such as the Fuel Characteristic Classification System (Ottmar et al. 2007) are beginning to incorporate fuel arrangement explicitly into fire behavior potential. Further development of these tools should incorporate feedbacks among fuel load, arrangement, and fine-fuel moisture to more accurately predict fire behavior. In practice, managers of forested lands can adjust their expectations of timelag response for fuel particles and beds to reflect significant delays in drying time as fuelbed loadings increase.

The research mentioned above is needed not only for the longleaf fuels studied here, but for other fuel types of interest. The wide range of timelags among treatments in the present study illustrates the potential for fuelbed architecture to dramatically affect expected fire behavior through modifications in moisture exchange—particularly after rain events, or possibly during prolonged dry periods.

## Acknowledgements

We give special thanks to Robert Mitchell, Matt McCorvey, Jason McGee, Matt Greene, and Jim Bradley for their help in data collection. This manuscript also was improved with the help of anonymous reviewers. Funding for

this project was provided by the Robert W. Woodruff Foundation and the Joseph W. Jones Ecological Research Center.

## References

- Anderson, H.E. 1990. Moisture diffusivity and response time in fine forest fuels. *Can. J. For. Res.* **20**: 315–325. doi:10.1139/X90-046.
- Anderson, H.E., Schuette, R.D., and Mutch, R.W. 1978. Timelag and equilibrium moisture content of ponderosa pine needles. USDA For. Serv. Intermountain For. Range Exp. Stn. Res. Pap. INT-202.
- Andrews, P.L., Bevins, C.D., and Seli, R.C. 2005. BehavePlus fire modeling system. Version 3.0. User's guide revised. USDA For. Serv. Rocky Mountain Res. Stn. GTR-106WWW. Revised.
- Blackmarr, W.H. 1971. Equilibrium moisture content of common fine fuels found in southeastern forests. USDA For. Serv. Southeast. For. Exp. Stn. Res. Pap. SE-74.
- Block, J.A. 1971. A theoretical and experimental study of nonpropagating free-burning fires. *In* Proceedings of the 13th International Symposium on Combustion, 23–29 August 1970, Salt Lake City, Utah. The Combustion Institute, Pittsburgh, Pa. pp. 971–978.
- Byram, G.M. 1963. An analysis of the drying process in forest fuel material. Paper presented at 1963 International Symposium on Humidity and Moisture, 20–23 May 1963, Washington, D.C.
- Florida Division of Forestry. 2007. 2007 Drought Action Plan. Florida Department of Agriculture and Consumer Services. Available from: <http://www.doacs.state.fl.us/press/2007/04162007.html> [accessed 10 January 2008].
- Fosberg, M.A. 1975. Heat and water vapor flux in conifer forest litter and duff: a theoretical model. USDA For. Serv. Rocky Mountain For. Range Exp. Stn. Res. Pap. RM-152.
- Fosberg, M.A. 1977. Heat and water transport properties in conifer duff and humus. USDA For. Serv. Rocky Mountain For. Range Exp. Stn. Res. Pap. RM-195.
- Holman, J.P. 1990. Heat transfer. 7th ed. McGraw-Hill, New York.
- Hough, W.A., and Albini, F.A. 1978. Predicting fire behavior in palmetto–gallberry fuel complexes. USDA For. Serv. Southeast. For. Exp. Stn. Res. Pap. SE-174.
- Incropera, F.P., and DeWitt, D.P. 1996. Fundamentals of heat and mass transfer. 6th ed. John Wiley and Sons, New York.
- Kreith, F. 1967. Principles of heat transfer. 2nd ed. International Textbook Co., Scranton.
- Linton, M. 1962. Report on moisture variation in forest fuels — prediction of moisture content. CSIRO Division of Physical Chemistry, Melbourne, Australia.
- Lyons, P.R.A., and Weber, R.O. 1993. Geometrical effects on flame spread rate for wildland fine fuels. *Comb. Sci. Technol.* **83**: 1–13.
- Mardini, J.A., Lavine, A.S., and Dhir, V.K. 1996. Heat and mass transfer in wooden dowels during a simulated fire: an experimental and analytical study. *Int. J. Heat Mass Transfer*, **39**: 2641–2651. doi:10.1016/0017-9310(95)00374-6.
- Modest, M.F. 1993. Radiative heat transfer. McGraw-Hill, New York.
- Nelson, R.M., Jr. 1969. Some factors affecting the moisture time-lags of woody materials. USDA For. Serv. Southeast. For. Exp. Stn. Res. Pap. SE-44.
- Nelson, R.M., Jr. 2001. Water relations of forest fuels. *In* Forest fires: behavior and ecological effects. Academic Press, San Diego, Calif. pp. 79–149.
- Nelson, R.M., Jr. 2003. Reaction times and burning rates for wind tunnel headfires. *Int. J. Wildland Fire*, **12**: 195–211. doi:10.1071/WF02041.
- Ottmar, R.D., Vihnanek, R.E., and Mathey, J.W. 2003. Stereo photo series for quantifying fuels. Vol. VIa. Sand hill, sand pine scrub, and hardwoods with white pine types in the Southeast United States with supplemental sites for Vol. VI. PMS 838. National Wildfire Coordinating Group, Boise, Id.
- Ottmar, R.D., Sandberg, D.V., Riccardi, C.L., and Prichard, S.J. 2007. An overview of the Fuel Characteristic Classification System — quantifying, classifying, and creating fuelbeds for resource planning. *Can. J. For. Res.* **37**: 2383–2393. doi:10.1139/X07-077.
- Rothermel, R.C. 1972. A mathematical model for predicting fire spread in wildland fuels. USDA For. Serv. Intermountain For. Range Exp. Stn. Res. Pap. INT-115.
- SAS Institute Inc. 2003. SAS/STAT and Base SAS. Release 9.1 for Windows. SAS Institute Inc., Cary, N.C.
- SigmaPlot. 1997. Transformations and regressions. SPSS Inc., Chicago, Ill.
- Steward, F.R. 1974. Fire spread through a fuel bed. *In* Heat transfer in fires: thermophysics social aspects economic impact. Scripta Book Co., Washington, D.C.
- Van Wagner, C.E. 1969. Drying rates of some fine forest fuels. *Fire Control Notes*, **12**: 5, 7, 12.
- Van Wagner, C.E. 1979. A laboratory study of weather effects on the drying rate of jack pine litter. *Can. J. For. Res.* **9**: 267–275. doi:10.1139/x79-044.
- Van Wagner, C.E. 1982. Initial moisture content and the exponential drying process. *Can. J. For. Res.* **12**: 90–92. doi:10.1139/x82-013.
- Vaz, G.C., André, J.C.S., and Viegas, D.X. 2004. Estimation of the radiation extinction coefficient of natural fuel beds. *Int. J. Wildland Fire*, **13**: 65–71. doi:10.1071/WF03009.
- Viney, N.R. 1992. Moisture diffusivity in forest fuels. *Int. J. Wildland Fire*, **2**: 161–168. doi:10.1071/WF920161.
- Weber, R.O., and De Mestre, N.J. 1990. Flame spread measurements on single ponderosa pine needles: effect of sample orientation and concurrent external flow. *Comb. Sci. Technol.* **70**: 17–32. doi:10.1080/00102209008951609.